Alt, J.C., Kinoshita, H., Stokking, L.B., and Michael, P.J. (Eds.), 1996
Proceedings of the Ocean Drilling Program, Scientific Results, Vol. 148

16. STRUCTURE OF THE SHEETED DIKE COMPLEX IN HOLE 504B (LEG 148)[1]

Yildirim Dilek,[2] Gregory D. Harper,[3] Philippe A. Pezard,[4] and Paola Tartarotti[5]

ABSTRACT

An additional 110.6 m of coring in Hole 504B on ODP Leg 148 recovered aphyric to phyric, massive diabasic rocks that are part of the lower sheeted dike complex of 5.9-m.y.-old oceanic crust. Structural studies of the drill core based on shipboard data and the analyses of geophysical downhole measurements show that fracturing was the main deformation process during the evolution of oceanic crust at Hole 504B. The existence in certain depth intervals in the core of zones of intense microfracturing suggests the occurrence of damage zones associated with faults or localized deformation zones. The majority of these microfractures have steep dips (>70°) and east-northeast strikes with subhorizontal slickenline lineations and are oblique to the orientation of the Costa Rica Rift and the modern horizontal principal stress directions. Open fractures in the core with shallow and steep dips are locally symmetric to the modern in situ stress field. Subhorizontal fractures observed in the drill core are absent on the borehole walls, as suggested by the FMS images, implying that they are drilling induced. A predominant fracture set defined by FMS images of the borehole has an average orientation of 052, 56°NW between 1900 and 2000 mbsf in the hole that is oblique to the Costa Rica Rift. The FMS and DLL-porosity logs suggest that a marked zone of subhorizontal fractures occurs at 1930 mbsf and an intense zone of vertical fractures at 2000 mbsf. Despite locally well-developed zones of fractures, fault rocks are rare in the drilled section of the hole and there is no evidence for any structural discontinuity in the core. Veins filled mainly with actinolite and chlorite seem to have formed as extension fractures and developed through syntaxial overgrowth of these vein-filling minerals on host-rock clinopyroxene along the fracture walls and/or by a succession of crack-seal increments. Steeply dipping veins striking east-southeast are commonly parallel to the dike margins and to the orientation of the Costa Rica Rift axis. Veins striking north-northeast are dike-orthogonal and might have formed as thermal contraction cracks during cooling of the dikes. Deformation in the lower sheeted dike complex at Hole 504B appears to be mainly brittle and limited to fracturing and veining.

INTRODUCTION

Deep Sea Drilling Project/Ocean Drilling Program (DSDP/ODP) Hole 504B is situated 200 km south of the Costa Rica Rift and midway between the Ecuador and Panama fracture zones and remains as the deepest basement hole in the oceanic crust (Fig. 1); Cann, Langseth, et al., 1983; Anderson, Honnorez, Becker, et al., 1985; Becker, Sakai, et al., 1988; Becker, 1989; Dick, Erzinger, Stokking, et al., 1992; Alt, Kinoshita, Stokking, et al., 1993). It penetrates 2.1 km into 5.9-m.y.-old oceanic crust and provides a significant in situ reference section for the physical and chemical structure of the upper oceanic lithosphere. The lithostratigraphy in the hole includes (Adamson, 1985), from top to bottom, sediments (274.5 m); an upper zone of pillow lavas, pillow breccias, hyaloclastites, flows, and sills (571.5 m); a transition zone of pillow lavas, flows, and dikes (209 m); and a lower zone of diabasic dike rocks (1055.6 m). Thus, the drilled section penetrates geophysically defined oceanic Layers 1, 2A, 2B, and 2C to a depth of 2.1 km beneath the seafloor (Alt, Kinoshita, Stokking, et al., 1993). Although a significant increase in the grain size of diabasic rocks has been observed in the cores recovered on Legs 140 and 148, the rocks are part of the sheeted dike complex; the dike/gabbro boundary is not yet reached in the hole. However, recent seismic studies in the area around Hole 504B and borehole seismic experiments at the hole indicate an important change in velocity gradient at about 1.2 ± 0.2 km depth similar to that commonly associated with the Layer 2/3 boundary and that seismic velocities steadily increase to a value of 6.8 km/s, typical of Layer 3, near 2060 meters below seafloor (mbsf) (Alt and the Leg 148 Scientific Party, 1993; Detrick et al., 1993). These findings and interpretations suggest that the Layer 2/3 boundary may lie within the dike complex and that it does not correspond to a major lithological change from dikes to gabbros (Detrick et al., 1994).

The alteration history of oceanic rocks recovered from Hole 504B and their geochemical and geophysical features have been extensively documented by previous DSDP and ODP research (e.g., Alt et al., 1985, 1986, 1989; Anderson, Honnorez, Becker, et al., 1985; Becker, Sakai, et al., 1988; Hobart et al., 1985; Honnorez et al., 1983; Morin et al., 1989, 1990; Newmark et al., 1985a; Newmark et al., 1985b; Pezard and Anderson, 1989). However, systematic structural studies of the drill core and combined analyses of structures observed and documented from core and borehole measurements have been limited (i.e., Agar, 1990, 1991; Dick, Erzinger, Stokking, et al., 1992; Agar and Marton, 1995). Such studies are crucial to constrain the deformation mechanisms and histories of in situ oceanic crust and thus have the potential to provide important information on the rheological properties of oceanic crust. Findings of the previous studies have shown that fracturing and brittle failure dominated the structural evolution of the oceanic crust drilled into at Site 504. Agar (1991) suggested that the fractures in the upper extrusive sequence were mostly related to thermal cracking due to cooling and to volume changes as a result of pervasive alteration of basalts. She reported the existence of a deformation zone in the basement based on observations in the discontinuous core record from the interval between 840 and 958.5 mbsf, where several discrete fault planes occur to be spatially associated with cataclastic zones, isoclinal microfolds, and alignment of

[1] Alt, J.C., Kinoshita, H., Stokking, L.B., and Michael, P.J. (Eds.), 1995. *Proc. ODP, Sci. Results,* 148: College Station, TX (Ocean Drilling Program).

[2] Department of Geology and Geography, Vassar College, Poughkeepsie, NY 12601, U.S.A. yidilek@vassar.edu

[3] Department of Geosciences, State University of New York at Albany, Albany, NY 12222, U.S.A. gdh@csc.albany.edu

[4] Laboratoire de Mesures en Forage, Institut Méditerranéen de Technologie, Technopôle de Château-Gombert, F-13451 Marseille Cedex 20, France; and Laboratoire de Pétrologie Magmatique, URA CNRS 1277, Faculté des Sciences et Techniques de Saint-Jérôme, Avenue Escadrille Normandie-Niemen, F-13397 Marseille Cedex 20, France. pezard@imtmer1.imt-mrs.fr

[5] Dipartimento di Geologia, Paleontologia e Geofisica, Università di Padova, Via Giotta 1, I-35157 Padova, Italy. tar@epidote.dmp.unipd.it

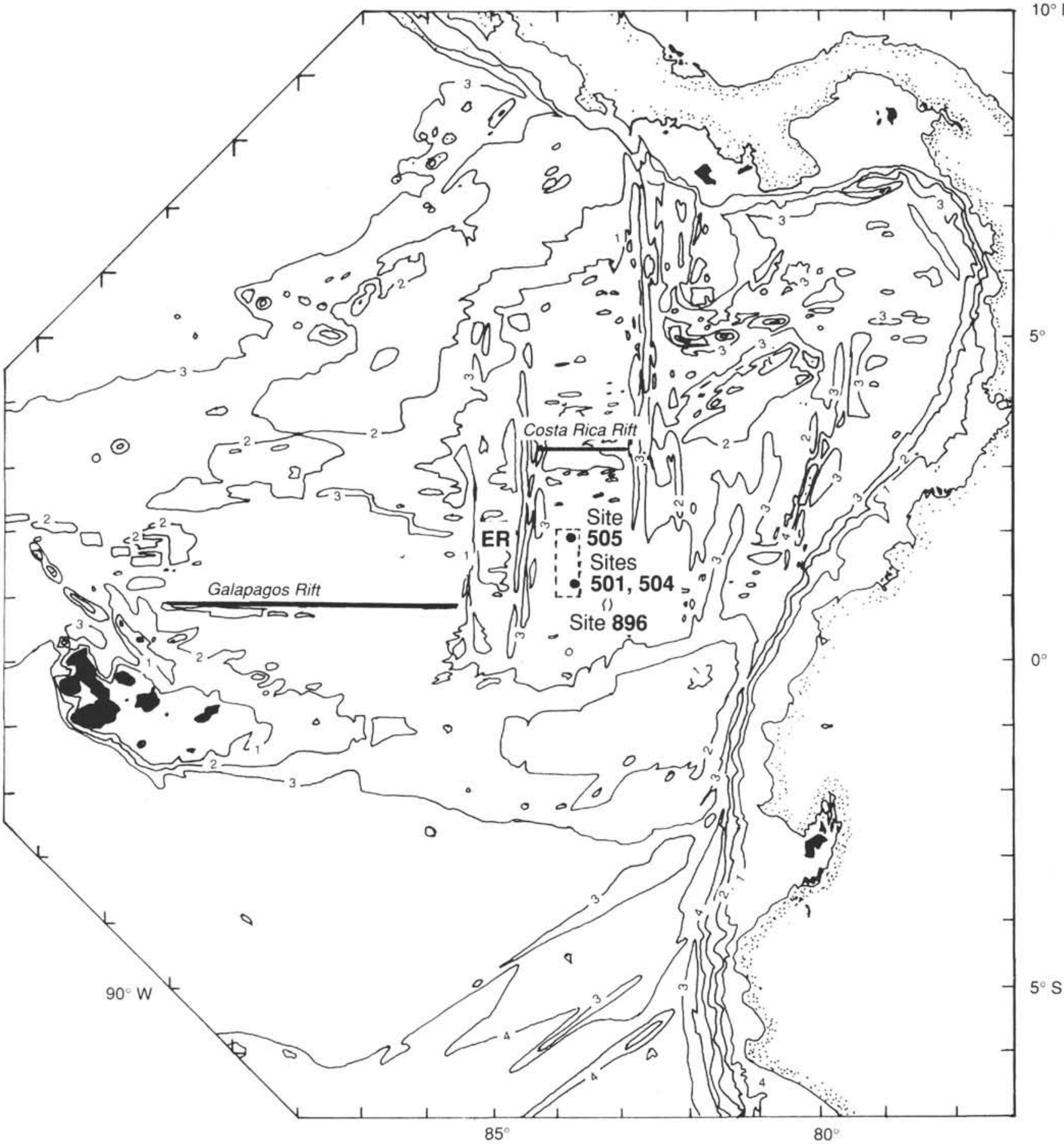

Figure 1. Location of DSDP Sites 501 and 505, DSDP/ODP Site 504, and ODP Site 896 south of the Costa Rica Rift in the eastern equatorial Pacific (after Hobart et al., 1985).

quartz and phyllosilicate minerals (Agar, 1991). This deformation zone lies at the top of the lithological transition zone between the extrusive sequence above and the dike complex below and thus coincides with a significant mechanical boundary in the basement. The stockwork zone of alteration between 910 and 930 mbsf in the oceanic crust occurs within this transition zone (Honnorez et al., 1985) and is possibly related to intense hydrothermal circulation facilitated by dilation during slip on shallow faults in the deformation zone (Agar and Marton, 1995). Diabasic dike rocks below the transition zone are relatively undeformed, and the structural evidence for brittle failure of the oceanic crust is limited to veins and microfractures as observed in the cores recovered from Hole 504B before Leg 148. Observed microfracture networks in dike rocks recovered during Leg 140 are interpreted, for example, to be related to thermal cracking along certain crystallographic planes (Agar and Marton, 1995).

Core observations and shorebased studies of the diabasic rocks recovered during Leg 148 show the existence of numerous closely spaced microfractures and zones of intense fracturing in the core. An increase in grain size of the rocks and an apparent decrease in the occurrence of chilled dike margins in the Leg 148 cores suggest higher temperatures and slower cooling rates near 2 km at depth during the evolution of the oceanic crust (Alt, Kinoshita, Stokking, et al., 1993) and may also point to the proximity of gabbros to the bottom of the hole at 2111.0 mbsf. During Leg148 a total of 110.6 m was cored with an average recovery of 10.4%, and a total of 25 lithological units was identified in mainly diabasic rocks. Drilling was stopped at 2111.0 mbsf when the drill string became stuck in the hole in a relatively soft zone with a high penetration rate (7 m/hr as opposed to 1 to 2 m/hr for the other dikes). Combined with the existence of highly fractured rocks near and at the bottom of the hole, this zone is interpreted as a fault zone at 2104–2111 mbsf (Alt, Kinoshita, Stokking, et al., 1993; Alt and the Leg 148 Scientific Party, 1993). It is probable that this inferred fault zone marks the boundary between the dikes above and gabbros below.

This paper focuses on the structure of the lower sheeted dike complex in Hole 504B and presents our observations and interpretations on the occurrence, nature, and mode of various structures between 2000.4 and 2111.0 mbsf based on core observations, borehole measurements, and shorebased studies associated with Leg 148. Comparison of the structures observed in the Leg 148 cores with those reported from the Leg 140 cores provides us with important information on their downhole variation and changes in structural styles with depth. The two major parts of the paper include the description of the occurrence and nature of mesoscopic and microscopic structures observed in the core samples and the structural analysis of the Formation MicroScanner (FMS, Schlumberger™) images obtained during Leg 148. This work represents the first attempt for a correlative analysis and interpretation of the drill core observations and FMS data from Hole 504B and complements the study of downhole measurements by Pezard et al. and Ayadi et al. in this volume. Attitudes of the oriented structures and the structural plots in this paper reflect the additional paleomagnetic measurements obtained during shorebased studies and the shipboard paleomagnetic measurements that were subsequently revised and corrected during the course of shorebased studies (S. Allerton, pers. comm., 1994). The "microfaults" as previously reported in Alt, Kinoshita, Stokking, et al. (1993) are also redefined as microfractures in this paper based on the findings of the shorebased studies.

STRUCTURAL CORE OBSERVATIONS

Diabases were recovered during Leg 148 at Hole 504B from depths between 2000.4 and 2111.0 mbsf in the lower sheeted dike complex (Alt, Kinoshita, Stokking, et al., 1993). The lithologies are mainly massive, homogeneous, aphyric to phyric diabase. All diabase samples show well-preserved primary (igneous) characteristics with no shape-fabric or preferred orientation of grains associated with crystal-plastic deformation. Major structures observed in the core include veins, fractures, igneous contacts, and cataclastic zones (Alt, Kinoshita, Stokking, et al., 1993).

Veins

Vein distribution and density in cores from Leg 148 are heterogeneous and vary from rare to intense (Alt, Kinoshita, Stokking, et al., 1993). There is no well-defined systematic set(s) of vein generations in the recovered core, and veins display different orientations and arrays. In thin sections veins range from 0.1 to about 2 mm in thickness with a maximal value of about 2.8 mm (i.e., Sample 148-504B-249R-1, 87–89 cm, Piece 27). They commonly occur as planar to curvilinear structures and appear sinuous in some cases (Samples 148-504B-251R-1, 28–30 cm, Piece 5, and 246R-1, 91–94 cm, Piece 26). Locally, they abut each other at high angles with no apparent displacements (Samples 148-504B-239R-1, 45–51 cm, Piece 14, and 246R-1, 21–25 cm, Piece 8), which is reminiscent of the shape and morphology of T-type joints of thermal-contraction origin in some intrusive and extrusive rocks (Fig. 2; Pollard and Aydin, 1988). Thinner veins generally merge into larger veins in many rock samples having moderate to intense vein density (e.g., Samples 148-504B-239R-1, 45–51 cm, Piece 14, and 245R-1, 21–24 cm, Piece 8).

Figure 2. Photomicrograph of two amphibole veins with a T-intersection. Fine-grained amphibole in the veins is associated with opaque seams (Sample 148-504B-249R-1, Piece 7).

The observed veins can be examined in three main groups based on the type of vein-filling minerals (Alt, Kinoshita, Stokking, et al., 1993). These include chlorite, actinolite (and actinolitic hornblende), and chlorite-actinolite veins. In addition, rare epidote and quartz-chlorite-sulfide veins occur in the core. The majority of chlorite veins have steep dips (75°–90°) and are commonly fractured (Fig. 3). The only two unfractured chlorite veins that were paleomagnetically reoriented display shallower dips (<25°). Actinolite veins are the most common vein types in the core and have variable dips with two main clusters at about 20°–25° and 85°–90°, showing a bimodal distribution similar to that observed in the Leg 140 cores (Fig. 4). Chlorite + actinolite veins commonly occur near chlorite-bearing veins and are similar in geometry and orientation. Both chlorite and actinolite veins have millimeter- to centimeter-scale alteration halos that are characterized by widespread replacement of the original mineral assemblages. The epidote and quartz-chlorite-sulfide veins have dips of 84° and 27°, respectively. The distribution of main vein types with different mineral fillings is locally heterogeneous. The moderately phyric plagioclase-olivine diabase rock (Unit 290) in Section 148-504B-249R-1 contains, for example, 16 chlorite and two actinolite veins (in a total of 25 pieces), whereas the moderately phyric plagioclase-olivine-clinopyroxene diabase rock (Units 291 and 293 combined) has 17 chlorite and 55 actinolite veins (in a total of 47 pieces).

Strikes and true dips of veins in samples corrected for the stable paleomagnetic declination show two main groups of vein orientation. One group has an east-southeast strike with steep dips, whereas the other group consists of veins with north-northeast strike and shallow to steep dips (Fig. 5). The east-southeast strike of the first group is parallel to the inferred dike azimuth and to the ridge axis of the Costa Rica Rift. The north-northeast strike of the second group is nearly orthogonal to the dike margins and may represent cooling fractures (Alt, Kinoshita, Stokking, et al., 1993). Similar vein orientations have been reported from the cores recovered during Legs 137 and 140 (Allerton et al., 1995).

Crosscutting relations between veins are scarce, and thus temporal relationships between different vein types are difficult to establish. In general, there are no significant shear displacements associated with the crosscutting veins although a few veins show offsets of much less than 1 mm (e.g., Samples 148-504B-246R-1, 91–94 cm, Piece 26, and 247R-1, 46–50 cm, Piece 12). Thin actinolite veins are oriented either subparallel or orthogonal to wider, major actinolite veins wherever they occur together. These thin veins commonly

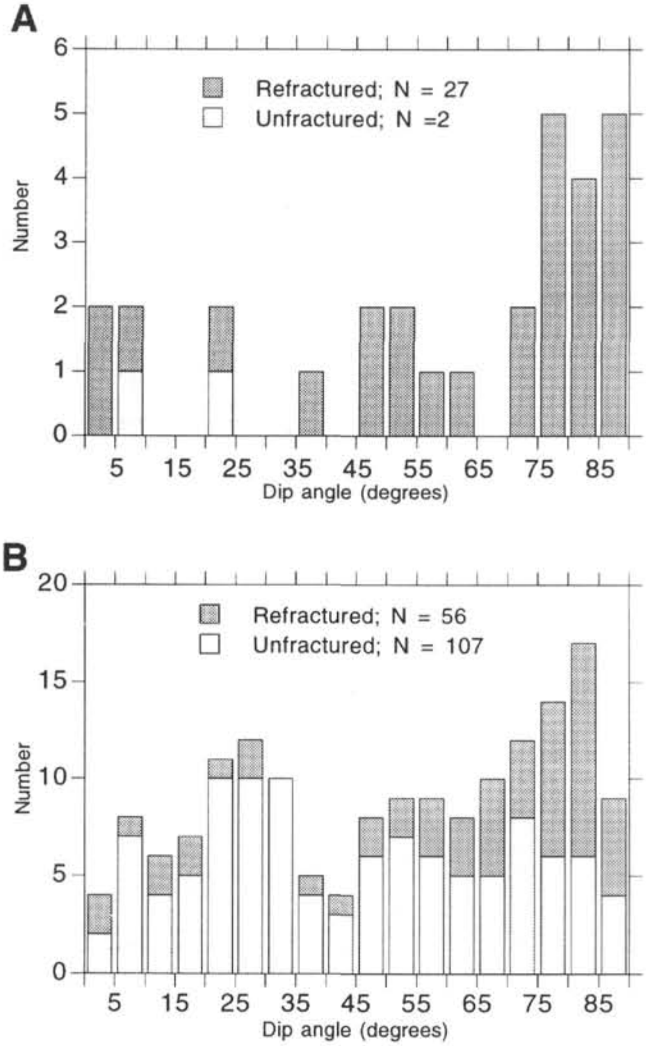

Figure 3. Dip histograms of refractured and unfractured chlorite veins in diabasic dike rocks in the cores from **(A)** Leg 148 and **(B)** Legs 140 and 148 combined (after Alt, Kinoshita, Stokking, et al., 1993).

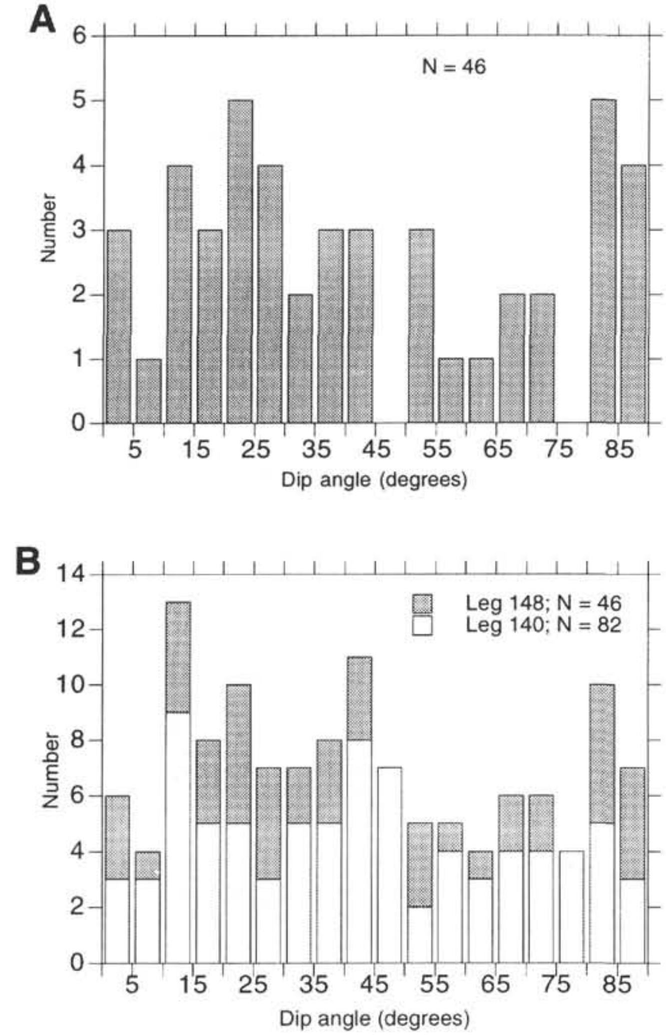

Figure 4. Dip histograms of actinolite veins in diabasic dike rocks in the cores from **(A)** Leg 148 and **(B)** Legs 140 and 148 combined (after Alt, Kinoshita, Stokking, et al., 1993).

cut across the wider veins and their alteration halos, suggesting later development than the wider ones (e.g., Sample 148-504B-245R-1, 21–24 cm, Piece 8). Thin veins are commonly filled with very fine actinolite fibers whereas wider ones are filled by coarser actinolite (Samples 148-504B-246R-1, 91–94 cm, Piece 26, and 247R-1, 46–50 cm, Piece 12). Actinolite veins and veinlets near dike margins are both subparallel and subperpendicular to the chilled margins. Limited observations suggest that dike-perpendicular veinlets crosscut the dike-parallel ones (i.e., Sample 148-504B-249R-1, 92–98 cm, Piece 28).

The internal fabric of the veins is controlled by the orientation of crystals and fibers of vein-filling minerals (Fig. 6). Fibers of actinolite and actinolitic hornblende are commonly perpendicular and/or oblique to the vein walls and become wider toward the center of the veins. The orientation of amphibole fibers may change, however, along the vein wall. This phenomenon seems to be controlled by the orientation of igneous minerals in the wall rock because the vein amphiboles are typically in optical continuity with amphibole pseudomorph after pyroxene in the groundmass. Thus, the shape and crystallographic fabric of the amphibole fibers reflect the orientation of the clinopyroxene in the wall rock, suggesting syntaxial overgrowth (Ramsay and Huber, 1983). Tartarotti et al. (1995) reported the occurrence of similar syntaxial overgrowth of amphibole fibers projecting from pyroxene grains in the wall rock of amphibole veins in the cores from Leg 140. The coarse amphibole fibers in the center of the veins are generally cut and/or replaced by extremely fine amphibole fibers (Fig. 7). These fine fibers are commonly randomly oriented, and their arrangement is not controlled by the orientation of amphiboles in the wall rock.

Some veins display internal deformation as indicated by bent and kinked coarse amphibole fibers (Samples 148-504B-239R-1, 45–51 cm, Piece 14; 250R-1, 57–60 cm, Piece 16; 251R-1, 28–30 cm, Piece 5; 242R-1, 28–33 cm, Piece 9; 246R-1, 1–94 cm, Piece 26; 246R-1, 111–115 cm, Piece 32; and 251R-1, 28–30 cm, Piece 5). Bent fibers are curved displaying wavy extinction, whereas kinks are generally restricted to coarser fibers (Fig. 8). In a few samples, fine fibers in the center of the vein are sheared and foliated (Fig. 6B; Samples 148-504B-245R-1, 21–24 cm, Piece 8; 249R-1, 134–138 cm, Piece 40; 251R-1, 28–30 cm, Piece 5; 249R-1, 87–89 cm, Piece 27; and 247R-1, 46–50 cm, Piece 12). Internal deformation of veins appears to be concentrated in samples at deeper crustal levels (from 2057.2 to 2090.2 mbsf). However, there is no evidence for deformation in the groundmass of the host rock of the veins, indicating that deformation is restricted to the veins. Both gently and steeply dipping veins exhibit deformed fibers suggesting that internal deformation does not show any relation with the vein orientation. We infer, therefore, that defor-

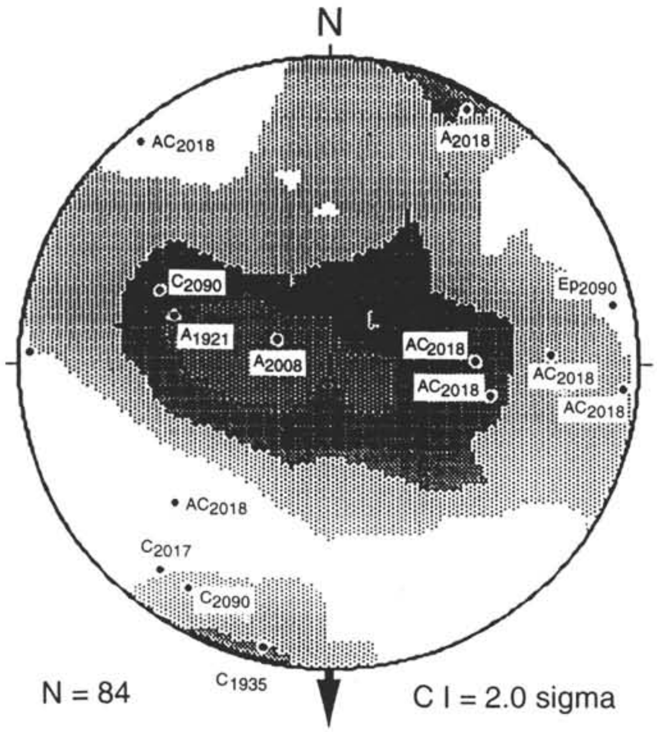

Figure 5. Poles to veins from Leg 148 superimposed on a Kamb contour plot of Leg 140 vein data. A = actinolite vein; AC = actinolite/chlorite vein; C = chlorite vein; Ep = epidote vein. Numbers refer to depth (mbsf). Arrow is the paleomagnetic reference direction used to correct the azimuths of the structural data. CI = contour interval.

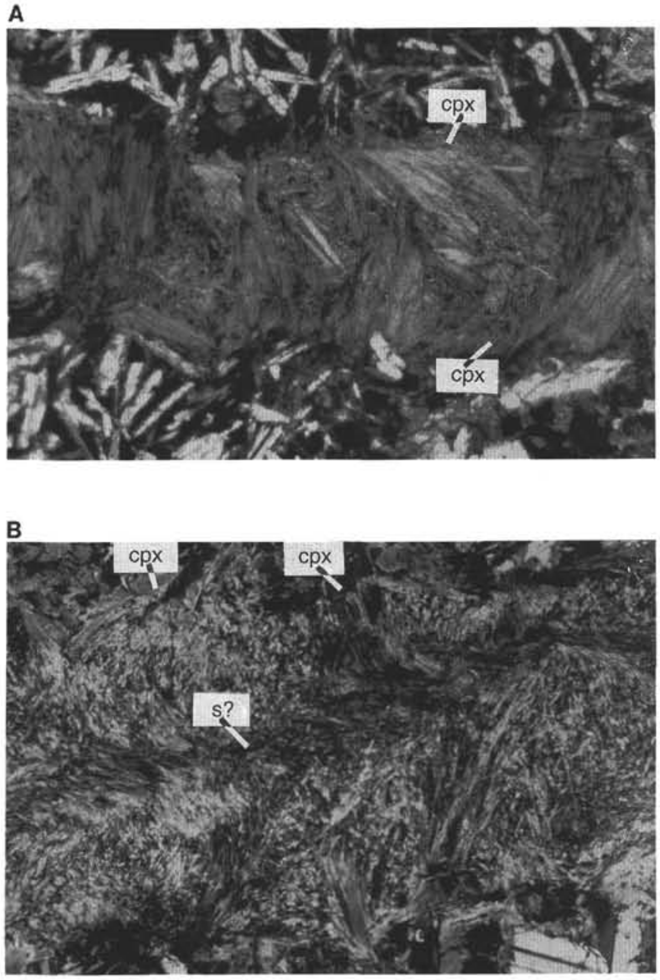

Figure 6. Photomicrographs of amphibole veins in diabasic dike rocks recovered from Hole 504B on Leg 148. Cpx = clinopyroxene; S = shear (?). **A.** Coarse-grained amphibole fibers with various directions of orientation. The orientation of fibers is strongly controlled by the crystallographic orientation of clinopyroxene grains in the wall rock through syntaxial overgrowth (Sample 148-504B-247R-1, Piece 11). **B.** Syntaxial replacement by amphibole of clinopyroxene in the wall rock. Strong preferred orientation of amphibole fibers in the center of the vein may point to deformation by simple shear. Sample 148-504B-249R-1, 134–138 cm.

mation was probably controlled by the internal fabric of the veins such that coarse fibers underwent kinking and bending while the very fine-grained mats of actinolite experienced shearing. Bending and kinking of the vein-filling fibers is most likely related to a local compressive regime, such as "collapsing" of the rock after fluids circulating in the veins have been discharged (Etheridge et al., 1984; Tartarotti et al., 1995). Alternatively, the deformation could be related to intraplate stresses that have produced strike-slip earthquakes in the region between the Cocos Ridge and the Peru-Chile trench (Bergman, 1986).

The morphology and internal fabric of the veins and the lack of displacement across them suggest that they formed as extensional displacements perpendicular to the fracture surface (mode I fracture of Pollard and Aydin, 1988). Some of these extensional veins might have subsequently been affected, however, by shear deformation (Samples 148-504B-245R-1, 21–24 cm, Piece 8; 249R-1, 87–89 cm, Piece 27; 249R-1, 134–138 cm, Piece 40; and 251R-1, 28–30 cm, Piece 5). The existence of step and staircase structures in some veins (e.g., 148-504B-246R-1, 111–115 cm, Piece 32) suggest, for example, that shearing displacement(s) might have accompanied opening displacements resulting in the generation of the mixtures of fracture modes I and II (Pollard and Aydin, 1988). Similarly, stair-shaped veins of the same inferred origin occur in the cores from Leg 140 (Tartarotti et al., 1995).

The fabric of coarse amphibole fibers in the veins suggests the operation of several processes during vein evolution. Syntaxial overgrowth of vein-filling amphibole is suggested by the existence of elongate actinolite fibers projecting away from the igneous clinopyroxene of the wall rock and into the veins (Fig. 6). This process is responsible for the diverse orientations of actinolite fibers along the walls within the vein because their shape and crystallographic fabric were controlled by the orientation of clinopyroxene grains and/or of their amphibole pseudomorphs along the vein edges in the host rock.

Another process that is commonly operative during the evolution of veins is the crack-seal mechanism whereby veins grow by repeated hydraulic fracturing followed by the precipitation of vein minerals (Ramsay, 1980; Ramsay and Huber, 1983; Tartarotti et al., 1995). Typical features of crack-seal veins include fibers oriented normal to the vein wall and vein-parallel bands of wall-rock and/or fluid inclusions. Locally, in some crack-seal veins the coarser amphibole fibers extend across the veins and tend to be oriented at a high angle to the vein walls. This amphibole fiber orientation appears to be controlled largely by the orientation of amphibole in the wall rock (pyroxene pseudomorphs). Thus, the coarse fibers linking the opposite vein walls are inferred to have nucleated on wall rock amphiboles. They subsequently grew away from the wall rock as the vein opened by successive crack-seal increments. The occurrence of very fine-grained fibrous amphibole filling the center of some veins suggests re-opening of veins by rupturing of the fibers along the center of the vein rather than by cracking along the vein walls (Fig. 7). The random arrangement of these very fine-grained fibers suggests that they grew freely inside the veins with no control on their orientation by wall rock or vein amphiboles (i.e., no syntaxial growth; Cox and Etheridge, 1983).

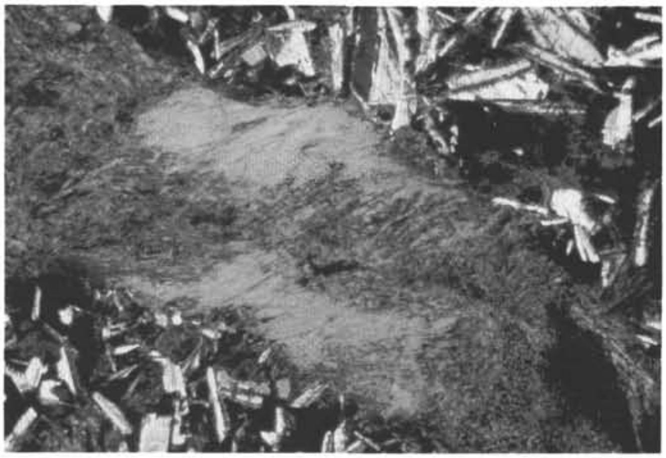

Figure 7. An amphibole vein with fine-grained fibers filling in the center and breaking through the coarse-grained, light-colored amphibole fibers (Sample 148-504B-247R-1, Piece 11).

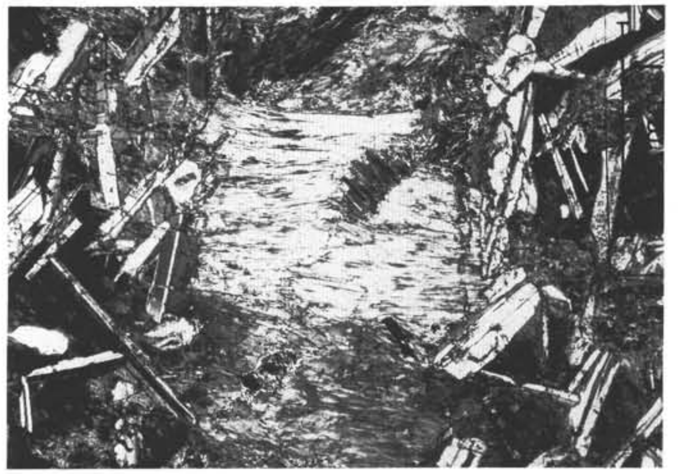

Figure 8. Crenulation of fibers in an amphibole vein suggesting shortening perpendicular to the vein walls (Sample 148-504B-246R-1, 111–115 cm, Piece 32).

Microfractures and Fractures

The numerous closely spaced microfractures observed in cores from Leg 148 (Fig. 9A) had not been previously seen in rocks of Hole 504B (J. Alt and S. Allerton, pers. comm.; 1993). The microfractures occurred in 11 of the 14 cores of Leg 148 and were especially abundant in Cores 242R-245R (2026–2052 mbsf) and in the junk basket at 2040 mbsf. An intense zone of fracturing is apparently present at the bottom of Hole 504B (2103–2111 mbsf) based on the presence of microfractures in the single piece recovered from the last core and in 10%–15% of the pieces in junk basket, the high rate of penetration during drilling, and extreme borehole instability. Individual pieces are commonly platy and were especially abundant in the junk basket at 2040 mbsf and in the core from 2026 to 2062 mbsf. Because most of the pieces containing microfractures are small and platy (core margins are not preserved), only 10 true dips of microfractures were obtained, most of which are more than 70°. Only four of these (all from the same piece) were oriented paleomagnetically with respect to azimuth, and all four strike east-northeast (Alt, Kinoshita, Stokking et al., 1993). Steeply dipping fracture surfaces have subhorizontal slickenline lineations (Sample 148-504B-246R-1, Pieces 12, 13, 19, and 20; 2052.6–2052.90 mbsf), whereas those with shallow dips display steeply plunging lineations (Sample 148-504B-241R-1, Piece 6; 2007.1 mbsf).

The microfracture surfaces are faintly lineated and occur as subparallel and/or anastomosing planes (Fig. 9A). They commonly show steep, subparallel slickenline lineations and subhorizontal step structures. Their spacing averages approximately 1 cm but can be on the order of a few millimeters in platy core pieces as recovered in junk baskets. The steps on the fracture surfaces are smooth, and their curvilinear traces are commonly orthogonal to the lineation (Fig. 9A). The sense of "offset" along the steps is consistent on the core face and on parallel faces of the same piece in the core, and in general these lineated fracture surfaces are analogous to the "P-T" structures of Petit (1987). P-T structures on fault surfaces in brittle rocks consist of striated shear fractures (P fracture surfaces) parallel to the main shear zone and unstriated planar fractures (T fracture surfaces) dipping at a shallow angle to the planes of P fractures. These P and T surfaces collectively form a dihedron the tip of which is commonly broken to form shallow steps that are generally ascending in the direction of the missing block of the fault or the shear zone (Petit, 1987). These features previously led us to interpret the fractures as microfaults (Alt, Kinoshita, Stokking, et al., 1993). However, no resolvable lateral offset or mineralization was evident in thin sections made on board during Leg 148, and we noted that these fractures may actually be joints with the lineated and stepped surfaces representing hackle marks formed during joint propagation (e.g., Engelder, 1987). Additional thin section observations and back-scattered electron imaging on the electron microprobe during shorebased studies (Fig. 9B) revealed no lateral offset or mineralization along the fractures, even at very high magnifications.

The significance of the microfractures in the Leg 148 core is uncertain, but they clearly represent extensional fracturing. The lack of any mineralization along the microfractures suggests a relatively young age, but the very small number of oriented samples and the large uncertainties in paleomagnetically corrected azimuths does not allow comparison with the modern (Morin et al., 1990) or ridge-related stress fields. Experimental and field studies in various rock types have shown the concentration of micro- and macrofractures in the vicinity of faults with an abrupt decrease in fracture and crack density away from the faults (Kanaori et al., 1991; Scholz et al., 1993; Anders and Wiltschko, 1994). This observation suggests that a wake of fractured rock (damage zone) develops adjacent to the fault as a zone of inelastic deformation (brittle process zone) when the fault is growing within the brittle field (Scholz et al., 1993). Systematic studies of microstructures in samples taken near thrust and normal faults have shown that microfracturing can develop without block rotation, recrystallization, extensive granulation, or crystal plasticity and that maximum microfracture density is independent of slip (Anders and Wiltschko, 1994). These relations are interpreted to indicate that the predominance of microfracturing occurs in proximity to the propagating fault tip. The microfractures observed in the Leg 148 core may therefore be related to fault zones (e.g., damage zone in vicinity of fault) and/or propagating fault tips, but evidence of shearing is virtually absent in the core. Recovery was generally very low, however, and fault rocks uncemented by secondary minerals are unlikely to have been recovered. Alternatively, the microfractures might have formed by hydrofracturing due to sudden changes in pore fluid pressures.

Fractures in the core with thicknesses less than 0.2 mm are commonly planar to sinuous, locally branching, and typically discontinuous (Alt, Kinoshita, Stokking, et al., 1993). More continuous, open fractures are generally wider (up to 0.5 mm) and commonly form broken faces on the core. Both incipient and well-developed open fractures display shallow and steep dips, similar to those observed in the Leg 140 core (Fig. 10). Fractures with shallow dips commonly have a saddle shape reminiscent of drilling- and coring-induced disk fractures as documented in other deep boreholes (Kulander et al:, 1990; Wolter et al., 1990; Roeckel et al., 1992). Steep to vertical fractures are common in the core, but they are probably under-represented because they are less likely to be intersected by vertical drilling. Some

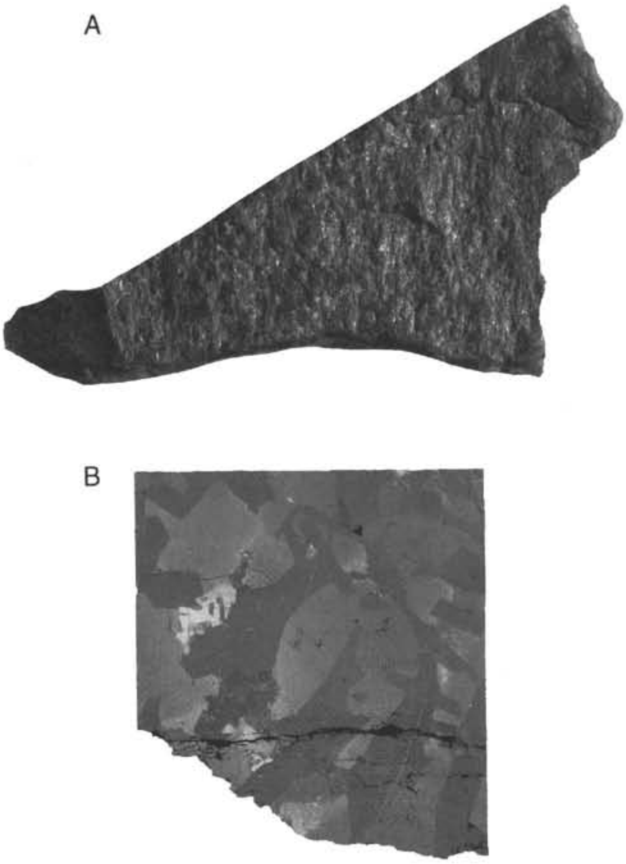

Figure 9. **A.** Diabasic dike rock with a microfracture surface having closely spaced, subparallel slickenline lineations and subhorizontal and curvilinear step structures. A chilled dike margin on the left is parallel to the lineations (Sample 148-504B-245R-1, 36–39 cm, Piece 13). **B.** Back-scattered electron imaging on the electron microprobe of a microfractured diabasic rock. The main fracture and the anastomosing, hairline fractures cut across the grains and grain boundaries with no displacement or shearing; there is no mineral filling in the fractures.

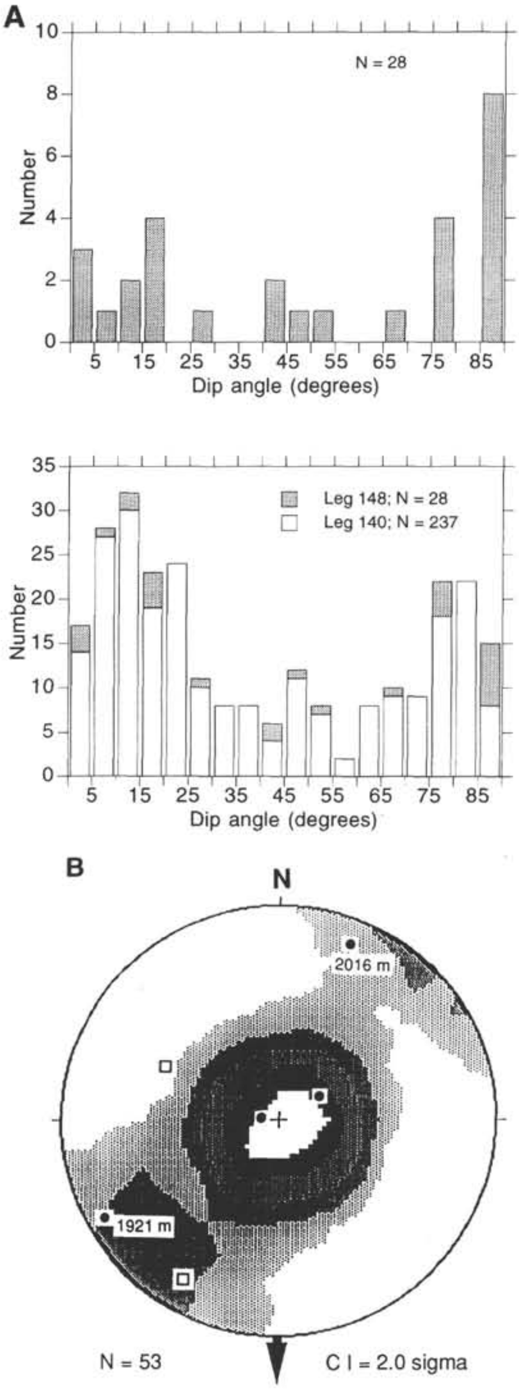

Figure 10. **A.** Histograms for true dip angles of fractures observed in the cores from Leg 148 (upper) and from both Legs 140 and 148 together (lower). **B.** Equal-area lower hemisphere projection showing poles to open fractures (solid circles) and refractured chlorite veins at 2090 mbsf (squares with solid circles) superimposed on a Kamb contour plot of Leg 140 fracture data. Numbers refer to depth as mbsf.

of the vertical fractures have chlorite coating on their inner walls, and they represent filled fractures and chlorite veins that were reopened during drilling.

The primary stress causing disking in the core may be associated with in situ stresses, unloading, and bit pressure assisted by torsional stresses and vibrations that accompany drilling and coring (Kulander et al., 1990). Systematic studies of saddle-shaped disks in the KTB (Kontinentales Tiefbohrprogrann Bundesrepublik) holes in Germany have shown that the trough axes of the disks are parallel to the maximum horizontal in situ stress (Roeckel et al., 1992). Paleomagnetically oriented open fractures in the Leg 148 core fall within the girdle defined by 55 oriented fractures from Leg 140 (Alt, Kinoshita, Stokking, et al., 1993) which is symmetric to the modern in situ stress field as determined from borehole televiewer measurements (Newmark et al., 1985a; Morin et al., 1990).

Igneous Contacts

Igneous contacts are represented by chilled dike margins between diabase dikes and are generally planar to curvilinear on a macroscopic scale (Fig. 9A; Alt, Kinoshita, Stokking, et al., 1993). They are rather irregular on a microscopic scale, however, with apophyses into the host rock and inclusions of the wall rock (i.e., Sample 148-504B-249R-1, 92–98 cm). Inclusions of host rock within the main body of the dike margin suggest a continued process of stopping and partial to complete(?) assimilation of small amounts of the wall rock. A microdike in Section 148-504B-241R-1, at 78–81 cm, has a tip terminating in a cataclastic zone, which includes a thin band (<1 mm) connecting an amphibole-filled vein and a thin (2 mm) portion of the chilled material. This cataclastic zone is made mainly of brecciated plagioclase clasts; both the chilled margin and the amphibole-bearing vein display a wide (2 cm) alteration halo.

The recovered chilled dike margins in the core are commonly spatially associated with veins and vein generations. Fine-grained actinolite (Sample 148-504B-245R-1, 36–39 cm) and epidote (Sample 148-504B-251R-1, 13–15 cm) veins occur parallel to and adjoining the drilled dike margins, which are bleached and altered. Actinolite veins at a high angle to the chilled margin form a second subset of veins associated with dike margins in the lower sections of the dike complex. These veins are less common, however, and rarely continue across the chilled margin and into the host rock.

Only three oriented dike margins were recovered during Leg 148 (see Fig. 14). The oriented chilled margins and the microdike have steep dips (76°–88°). One paleomagnetically oriented dike margin (Sample 148-504B-251R, 13–15 cm, Piece 4) has a strike of 118° that is subparallel to the ridge axis of the Costa Rica Rift; it dips 84° to the south, away from the ridge axis.

Cataclastic Zones

Cataclastic zones are rare in the core and are spatially and temporally associated with veins and chilled dike margins (Alt, Kinoshita, Stokking, et al., 1993). They are submillimetric to millimetric in scale, and they contain fine-grained and brecciated plagioclase and amphibole grains in narrow bands (i.e., Samples 148-504B-245R-1, 36–38 cm, and 241R-1, 78–81 cm). Locally, the host rock near the cataclastic zones is deformed as evidenced by the presence of bent and broken mineral grains. Evidence for incipient cataclasis is seen in Sample 148-504B-251R-1, 28–30 cm, where grain-size reduction of plagioclase and amphibole occurs in a braided network of converging veins.

STRUCTURAL DATA FROM DOWNHOLE MEASUREMENTS

The Formation MicroScanner (FMS, Schlumberger™) produces electrical images of the borehole surface by mapping its conductivity and resistivity using an array of small, pad-mounted electrodes (Lüthi and Banavar, 1988; Pezard et al., this volume). The FMS tool designed for ODP borehole measurements utilizes four pads furnished with 16 electrodes, and a current flows from each electrode to a single return electrode located at the top of the sonde during logging runs. The imaging depth into the borehole walls is relatively shallow (several centimeters) due to the geometry of the electrodes; however, the sampling rate of the FMS is about 2.5 mm giving a resolution on the order of 1 cm, and thus thin features (down to a few micrometers) that have a conductivity contrast to their host rock may be detected by the FMS.

The techniques and methods of data processing and image analysis from Leg 148 downhole measurements in the lower part of Hole 504B are explained in Ayadi et al. (this volume) and Pezard et al. (this volume). Mapping fractures on FMS images involve identifying traces that display a conductivity contrast to the surrounding rock. A best-fit sinusoid through these traces on the four images defines a planar feature with a dip angle (related to the amplitude of the sinusoid) and dip direction (given by the lowermost point of the trace). Commonly, traces with dip angles up to 80° to 85° are depicted on all four images, whereas near vertical traces can only be visible on one image.

The FMS data and analysis from the lower part of Hole 504B are also complemented by the resistivity data recorded with the Dual Laterolog (DLL) tool of Schlumberger (Ayadi et al., this volume; Pezard et al., this volume). This lateral device measures the horizontal electrical resistivity of the rock along the borehole walls which is in turn used to estimate the total porosity and distribution of fractures in the borehole walls. Combination of the FMS and DLL data and analyses provides significant information on fracture orientation and porosity.

The orientation of 4428 planar features was interpreted from images made with the Formation MicroScanner (Pezard et al., this volume) for the depth range of 1900–2079 mbsf (Fig. 11). This data set represents more than two orders of magnitude more data than available from measurements made directly on the core. Core measurements consist of only 14 veins and three fractures between 2000.4 and 2111.0 mbsf that have azimuths corrected paleomagnetically (only 3 veins and one fracture from 1900 to 2000 mbsf; Dick, Erzinger, Stokking, et al., 1992; Alt, Kinoshita, Stokking et al., 1993). The number of planar features imaged by FMS averages between 20 and 25 per meter. A stereoplot of all planar features imaged by FMS is shown in Figure 12, and stereoplots for individual depth intervals are shown in Figure 13. The boundaries of these intervals correspond to relatively abrupt changes in the dominant orientation of planar features between 1900 and 2000 mbsf; below 2000 mbsf they were chosen to correspond to depths sampled in drill cores to facilitate comparison with structures measured in the cores from Leg 148. This is a different approach from that of Ayadi et al. (this volume), who classified the FMS generated fractures based on their dip angles. They identified four subgroups of fractures between 1900 and 2079

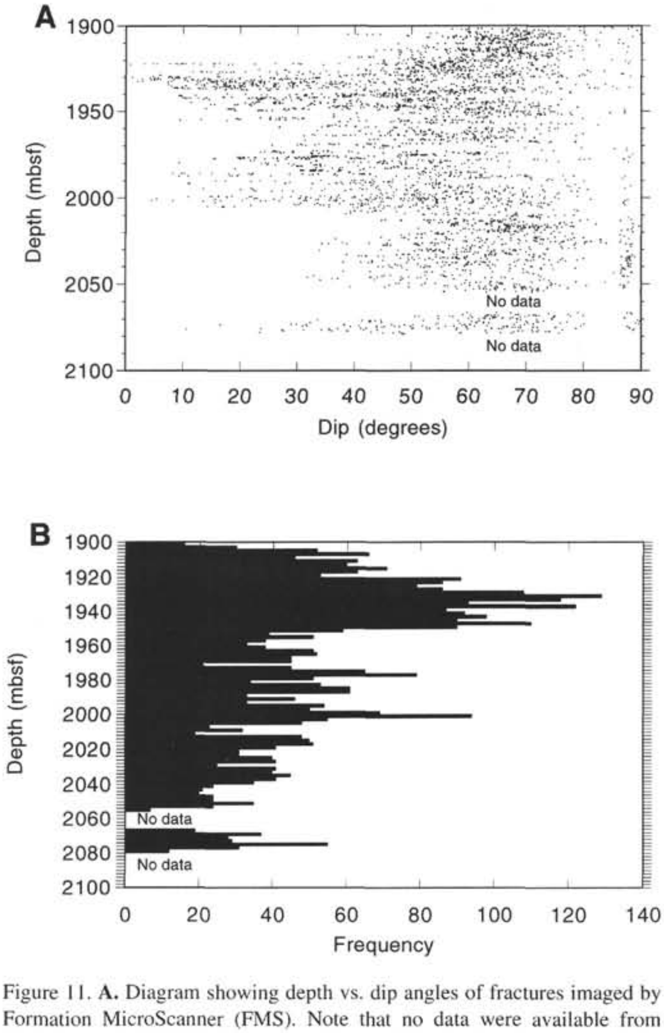

Figure 11. **A.** Diagram showing depth vs. dip angles of fractures imaged by Formation MicroScanner (FMS). Note that no data were available from depth intervals 2055–2065 mbsf and from 2080 mbsf to the bottom of the hole. Majority of the FMS-imaged fractures have moderate to shallow dips at 1930 and 2000 mbsf. **B.** Depth vs. frequency of FMS-depicted fractures in Hole 504B.

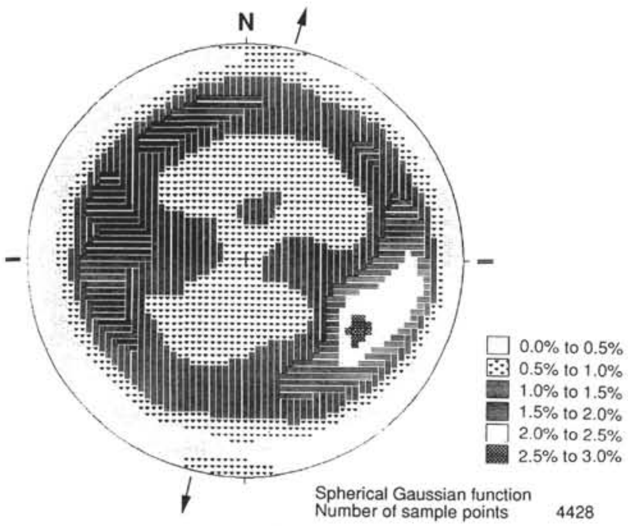

Figure 12. Contour diagram of all planes imaged by FMS between 1900 and 2079 mbsf in Hole 504B. The nearly east-west trending double lines mark the orientation of the Cocos Ridge; north-northeast-oriented outward pointing arrows represent the long axis of borehole breakouts from 1942 to 1979 mbsf.

mbsf with dips ranging from subhorizontal (<30°), intermediate (30°–60°), subvertical (60°–85°), to steep (>85°), and they described five zones between 1900 and 2079 mbsf in which one or more subgroups of fractures with different dip angles occur. Although based on an arbitrary selection, this approach is useful for comparison of FMS-derived fracture density profiles to those obtained from the DLL data and it complements the fracture analysis and the comparison of core observations with the FMS data presented in our study.

The planar features imaged with the FMS data are interpreted to represent open fractures on the borehole wall (Pezard et al., this volume). Figures 11 and 12 depict depth vs. dip angles and frequency, and a contour diagram of these inferred fracture planes. A fracture set with an average strike and dip of 052°, 56° NW (Fig. 13) is dominant between 1900–2000 mbsf and is present at all depths except for 1922–1924 and 1929–1938 mbsf, where shallow dips are predominant (Fig. 13). Other moderately dipping fracture sets are common but are restricted to certain depth intervals. Except for a few depth intervals, more than one fracture set is generally present, but four or more sets may be present over depth intervals of only a few meters (e.g., Fig. 13L).

It is important to note that structural data derived from a vertical drill hole will be strongly biased toward lower dips. This bias is clearly evident in measurements of veins and fractures in the core (Dick, Erzinger, Stokking, et al., 1992; Alt, Kinoshita, Stokking, et al., 1993), in plots of planes imaged from FMS data (note abrupt drop off for dips greater than 70° in the dip-vs.-depth plot of Fig. 11A and in the fracture frequency-vs.-depth plot (Fig. 11B) that shows a much higher frequency where subhorizontal fractures are present (e.g., 1929–1938 mbsf).

COMPARISON OF FMS DATA WITH STRUCTURES IN DRILL CORE

Comparison of the FMS data with observed structures in drill core from Leg 148 is adversely affected by the low core recovery and many small unoriented pieces recovered during drilling, the low number of structures in the core for which azimuths have been corrected paleomagnetically, and the large uncertainties of these corrected azimuths due to secular variation of the Earth's magnetic field. In addition, the assigned depth of a particular piece of the core is accurate only to a within a few meters as a result of the irresolution of the depth (within several meters) of the FMS tool relative to the core. Nevertheless, a comparison of the FMS data with the core observations gives us an opportunity to correlate the mode and nature of the structures (particularly fractures) observed in the core and in the borehole walls and hence to document the fracture porosity in the basement.

Veins

True dip data from Legs 137, 140, and 148 show a dominance of subvertical and gentle to subhorizontal dips of the veins in the core (Dick, Erzinger, Stokking, et al., 1992; Alt, Kinoshita, Stokking, et al., 1993). A contoured stereoplot of poles of oriented veins from the Leg 140 cores is shown in Figure 5, along with individual poles to veins from 1900 to 2111 mbsf. The subvertical set strikes west-northwest, and the second set strikes dominantly north-northeast with a strong maximum corresponding to subhorizontal dips.

The abundance of subhorizontal to gently dipping veins contrasts strongly with the near absence of these orientations for planes imaged by FMS outside the zone from 1922 to 1939 mbsf. Only one gently and one steeply dipping vein were obtained from the drill core for these depths. Although there appears in some zones to be similarly oriented girdles defined by poles to planes in the FMS data (1939.5–1950, 1980–1990, 1994–1996.5 mbsf), the near absence of subhorizontal planes in the FMS data (except locally) strongly suggests that the planes imaged using the Formation MicroScanner are not veins. This may be due to the fact that actinolite and chlorite minerals that fill the veins do not have sufficiently different resistivity from the host diabase. Alternatively, only open fractures might have been mapped by the FMS images, perhaps because they show the greatest contrast due to the high conductivity of seawater.

Fractures

Fractures in the drill core of Legs 140 and 148 are bimodal, consisting of a horizontal to gently dipping set having no preferred strike and a steeply dipping set striking west-northwest (Fig. 10; Dick, Erzinger, Stokking, et al., 1992; Alt, Kinoshita, Stokking et al., 1993). In contrast, gently dipping planes imaged by FMS generally occur only locally, primarily in the intervals at 1922–1924 and 1929–1938 and, to a lesser extent, at 1998–2003 mbsf (Fig. 11A). The presence of abundant subhorizontal fractures in the drill core but not in the drill hole is readily explained by drilling-induced disk fractures that result from in situ stresses, unloading of the overlying rock column, and bit pressure (Kulander et al., 1990). Disk fractures may be spaced on the order of 10 cm, resulting in disk-shaped fragments that commonly have a medial saddle. Such disks occur in the lower part of Hole 504B (Dick, Erzinger, Stokking, et al., 1992; Alt, Kinoshita, Stokking, et al., 1993), and disk fracturing is probably largely responsible for the paucity of continuous core and abundance of small pieces.

A plot of depth vs. dips of planes imaged by FMS (Fig. 11A) for 1900–2079 mbsf shows a distinct set of subvertical planes that may correlate with west-northwest vertical fractures observed in the drill core (Fig. 10B). There is a clustering of the strikes of the subvertical FMS planes at 80°–100° (Fig. 14). For comparison, the strike of oriented, steeply dipping (>70°) fractures observed in the drill core are also shown in Figure 14. There are very few data from the core, but five of the eight open fractures, which include refractured chlorite veins, have strikes similar to those of the subvertical FMS planes, although they generally strike 10°–15° more easterly.

The steeply dipping fractures in the Legs 140 and 148 drill core have been interpreted as drilling-induced based on comparison with other deep drill holes (Dick, Erzinger, Stokking, et al., 1992; Alt, Kinoshita, Stokking, et al., 1993). Such steeply dipping, drilling-induced fractures tend to occur near the center of the core, but commonly curve upward to dip from 30° to 75° at the core boundary (Ku-

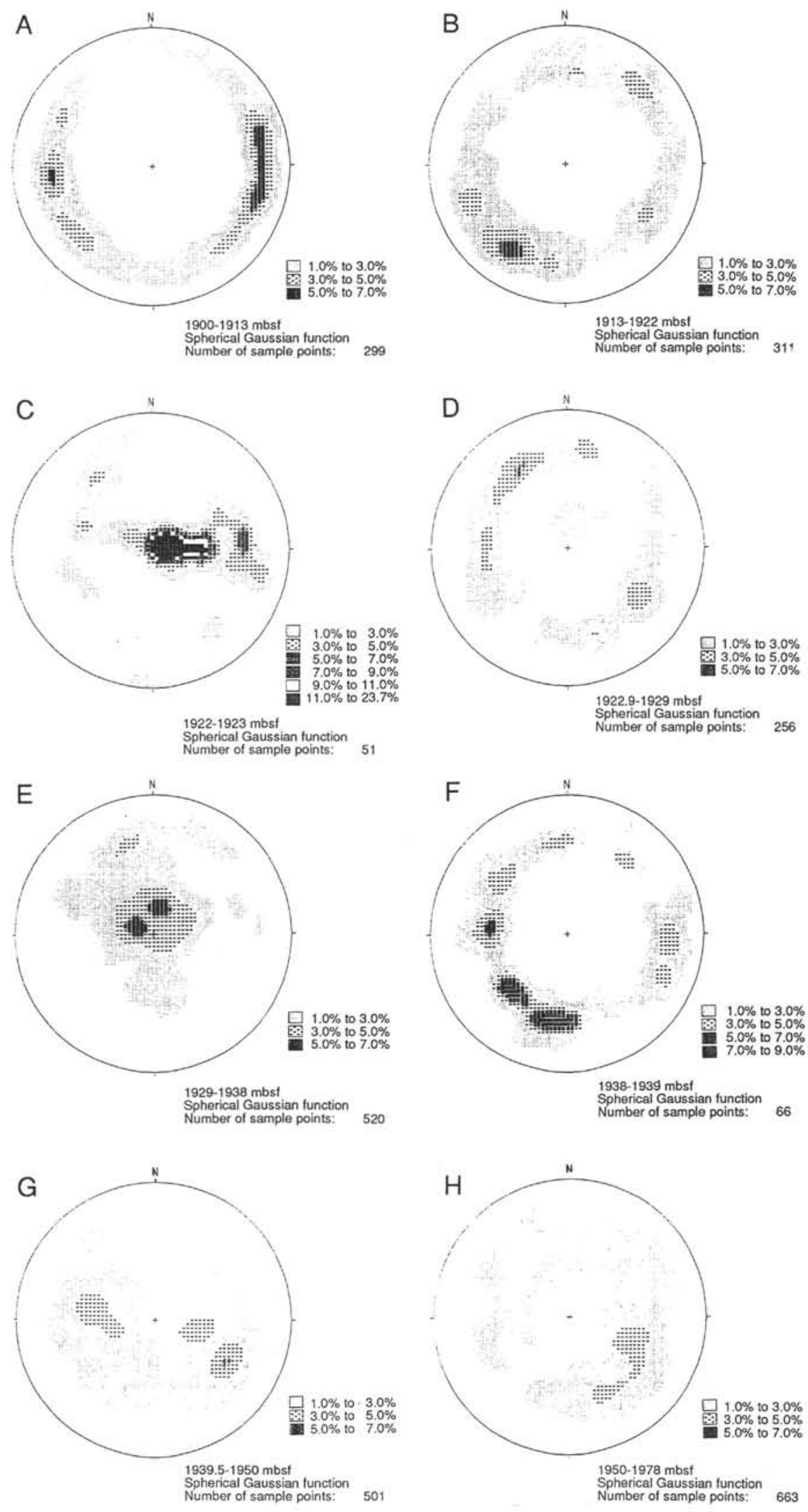

Figure 13. Contour diagrams of all planar features imaged by FMS in sequential depth intervals from **(A)** 1900 mbsf down to **(T)** 2079 mbsf in Hole 504B. Figure13P also shows poles to four microfractures from Core 148-504B-240R (Piece 6). See text for discussion and interpretation.

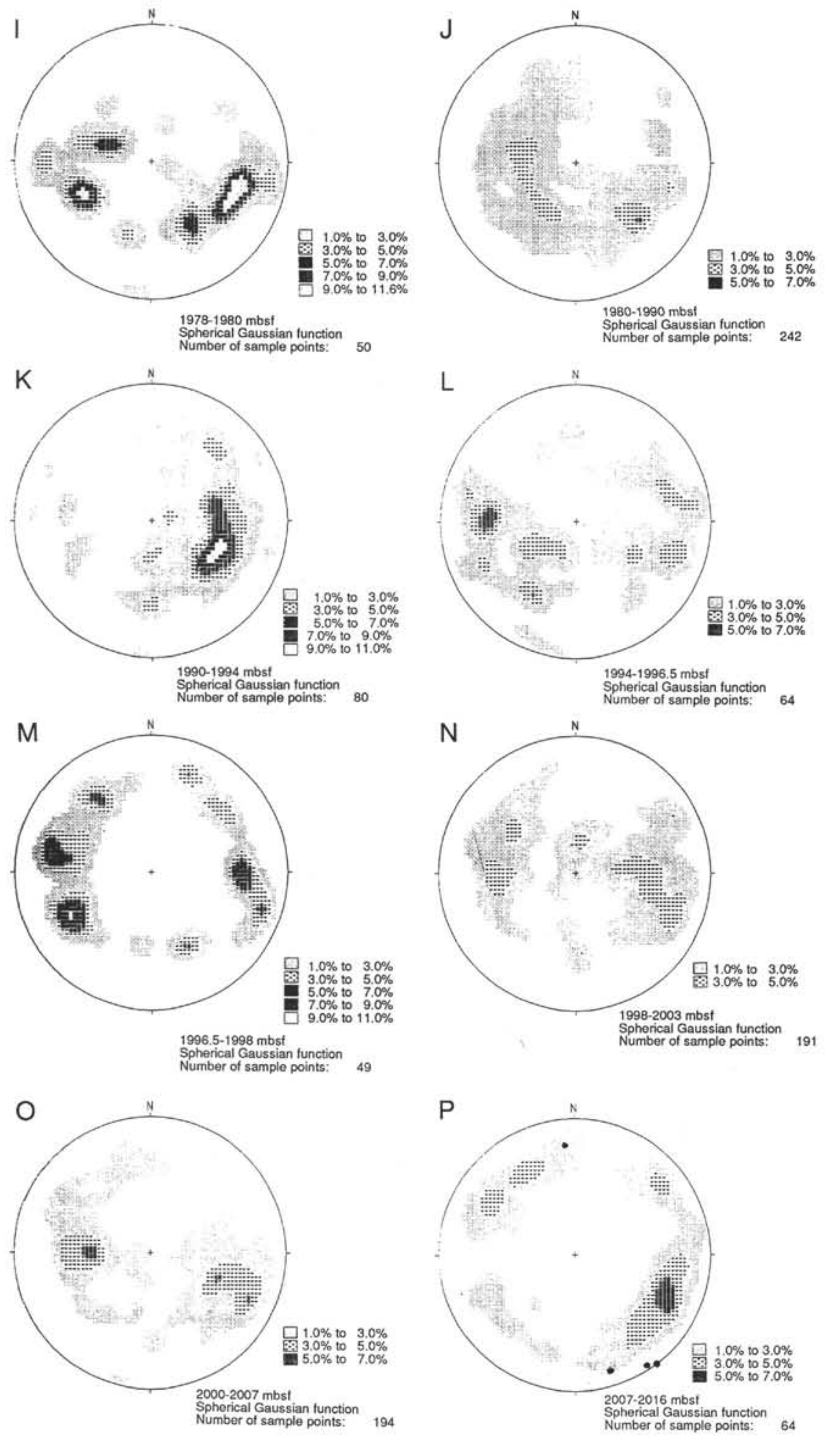

Figure 13 (continued).

lander et al., 1990); it has been inferred that these petal-shaped fractures form below the drill bit and extend into the rock beyond the perimeter of the drill bit. The strike of petal fractures appears to be parallel to local or perhaps regional in situ stress, and petal fractures would be evident in the walls of the drill hole. The strike of the subvertical planes (80°–100°) is approximately normal to the long axis of borehole breakouts occurring between 1940 and 2075 mbsf (Fig. 14; Alt, Kinoshita, Stokking, et al., 1993). In light of these characteristics, the subvertical fractures in the FMS images are most likely drilling-induced. Interpretation of the subvertical fractures as drilling-induced extension fractures is consistent with the stress field implied from the borehole breakouts (Fig. 14) in that the minimum horizontal stress direction is generally parallel to the elongation of the borehole and normal to the strike of vertical drilling-induced frac-

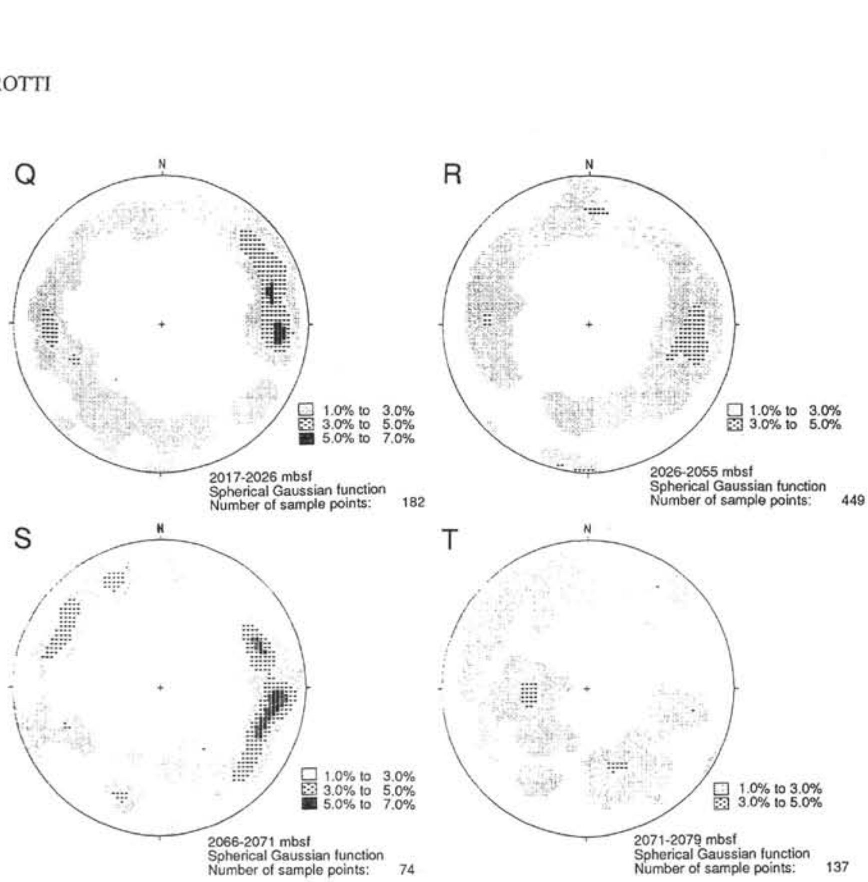

Figure 13 (continued).

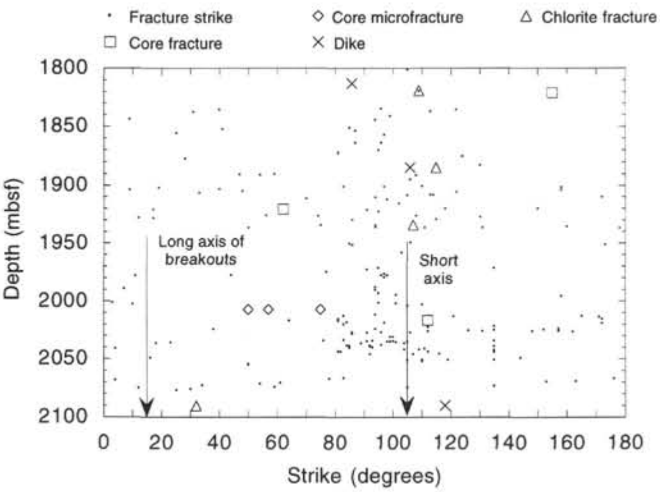

Figure 14. A composite depth vs. strike diagram showing the strikes of subvertical (>70°) FMS-depicted fractures together with oriented subvertical (>70°) fractures and microfractures observed in the drill core, refractured chlorite veins, and dike margins. Strikes of the long and short axes of borehole breakouts are also shown for reference.

tures. The only problem with this interpretation is that the petal shape of such drilling-induced fractures predicts that they should dip from 30° to 75° toward the drill hole (Kulander et al., 1990) rather than being nearly vertical as in the FMS images. Little, if any, curvature of probable drilling induced center-line fractures was observed in the Leg 148 cores, so that values closer to vertical would be expected in the core walls.

An alternative interpretation is that the east-west-striking, vertical, and/or the south-dipping fracture sets imaged using FMS data are natural. They strike parallel to the Costa Rica Ridge axis and to lineated bathymetry in the vicinity of Hole 504B, and the south-dipping set dips in the same direction as dike margins in the drill core (Dick, Erzinger, Stokking, et al., 1992; Alt, Kinoshita, Stokking, et al., 1993). Dike-parallel joints are probably formed by thermal contraction during dike cooling and are common in dike complexes in ophiolites. If the east-west-striking fractures are natural, then the strongest fracture set, corresponding to an average strike and dip of 52°, 56° northwest, and possibly the fracture set having a similar strike but southeast dip (Fig. 12), could be interpreted as drilling-induced petal centerline fractures. Although this would be consistent with the predicted dips of petal fractures in the borehole walls (Kulander et al., 1990), these fractures strike subparallel rather than orthogonal to the minimum horizontal stress inferred from borehole breakouts (Fig. 14; Morin et al., 1990; Alt, Kinoshita, Stokking, et al., 1993).

Microfractures

The closely spaced microfractures that were recovered in the drill core and in the junk baskets below 2000 mbsf are open fractures that should be visible on the FMS images. The centimeter-scale spacing is close enough that they should commonly be found in the bore hole walls despite their steep dip angles (10 oriented microfractures all have dips more than 70°). The poles to four microfractures from Piece 6 of Core 240R are plotted in Figure 13P, superimposed on a contoured diagram of poles to 176 fractures imaged by FMS for the depth interval corresponding to Core 240R (2006.9–2016.5 mbsf). The poles to microfractures from the core plot reasonably close to the two maxima corresponding to steeply north-northwest and east-southeast dipping planes. The drill cores containing the highest percentages of pieces having microfractures (Cores 242R–247R; 2026.5–2055.0 mbsf) are characterized by four maxima of FMS-derived fractures corresponding to steep dips toward the east, west, and south, and an east-striking (drilling induced?) subvertical set (Fig. 13R; no FMS data for depths of Core 248R). Core 249R (2071–2080 mbsf) also contains microfractures, but a plot of the FMS-derived fractures for this depth interval (Fig. 13T) shows a number of weak maxima corresponding to moderate dips at variable strikes. However, the vertical fracture porosity calculated from the dual laterolog (DLL) electrical resistivity sonde is relatively low, and borehole breakouts are relatively rare over this depth interval (Fig. 15).

All of the cores containing microfractures have no or few subhorizontal planes imaged from FMS data at equivalent depths (Figs. 13N–13T); it is thus reasonable to conclude that virtually all FMS depicted fractures have moderate to steep dips, consistent with the sparse true dip data from the core. Plots of fractures imaged from FMS data for the two cores from Leg 148 containing no microfractures do not appear to be appreciably different (Figs. 13Q, 13S). In summary, the limited fracture orientations from the drill core are consistent with the FMS-derived fracture orientations; however, the fractures observed in the core cannot be assigned unequivocally to one or more of the FMS fracture sets.

Variation of Fracture Orientation with Depth

The vertical and horizontal DLL-derived porosity logs, which sample on the scale of 1 m, clearly show two zones of intense fracturing in the vicinity of 1930 and 2000 mbsf (Fig. 15). The upper zone is dominated by subhorizontal fractures and is identified from DLL resistivity measurements as a high porosity region (Ayadi et al., this volume). This is consistent with the fracture orientations derived from the FMS data, which show two zones at 1922–1923.8 and 1929–1938 mbsf consisting almost entirely of subhorizontal to gently dipping fractures (Figs. 12, 13C, 13E). Dips are predominantly to the west between 1929 and 1938 mbsf and vary from east-southeast through southwest between 1922 and 1923.8 mbsf with a secondary maximum corresponding to fractures dipping moderately toward the south-southeast. These two zones are separated by an interval dominated by moderately dipping fractures of variable strikes, similar to those above 1938 and below 1922 mbsf (Fig. 13L), but also containing some fractures dipping gently toward the south (Fig. 13D). This interval of subhorizontal fractures around 1930 mbsf nearly coincides with the site of a significant change in hole deviation at 1950 mbsf and with the site of a P-wave velocity decrease (Pezard et al., this volume).

The DLL-derived fracture porosity indicates that the highly fractured zone at about 2000 mbsf is dominated by vertical fractures. This is verified by the poles to fractures imaged with FMS data; this zone between 1980 and 2003 mbsf has been divided into five subdomains based on changes in fracture orientations (Figs. 13K–13N). Note that the gently south-dipping fractures present between 1988 and 2003 mbsf (Fig. 13N) are similar to those between 1922 and 1938 mbsf (Figs. 13C, 13E). The other subdomains have several distinct fracture sets, similar in orientation to those above and below this zone, but northwest-dipping fractures dominate the interval from 1990 to 1994 mbsf.

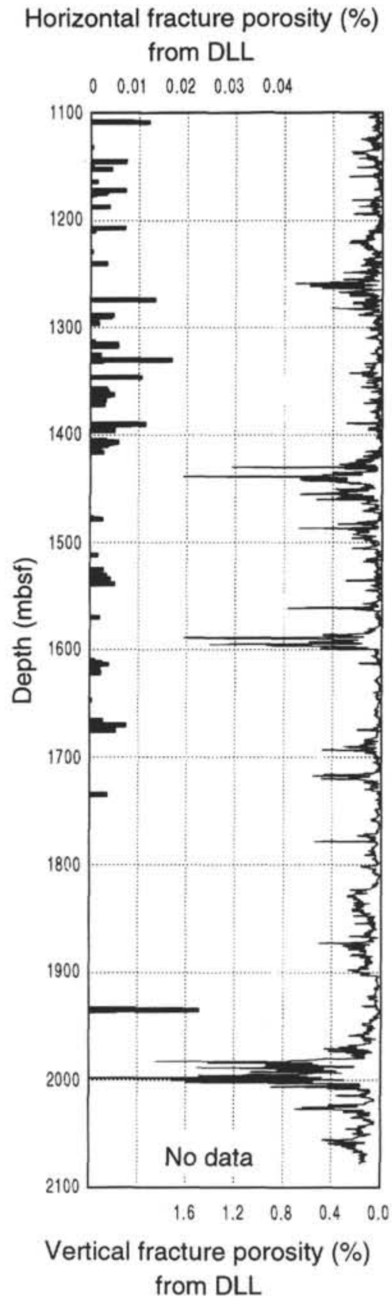

Figure 15. Distribution of the horizontal and vertical fracture porosity in Hole 504B calculated from the dual laterolog (DLL).

DISCUSSION

The fracture analysis based on the correlation of core observations and FMS data suggests that steep to subvertical fractures near the bottom of Hole 504B (bottom 167 m) are open fractures that were most likely developed as a result of drilling operations. The orientation of these fractures coincides with the azimuth direction of borehole enlargements which in turn corresponds to the direction of maximum horizontal stress (SH_{max}) determined from BHTV image analysis higher in the hole (Morin et al., 1990; Pezard et al., this volume). These fractures and borehole enlargements are probably related to thermal fracturing associated with induced cooling of the hole before drilling at the beginning of Leg 148 (Pezard et al., this volume).

One of the major questions regarding the FMS-derived fracture data is whether any of the intensely fractured intervals represent a fault zone. Intensely fractured zones, such as those at depths near 1930 and 2000 mbsf, evident in both the FMS and DLL logs could be either faults or simply zones having a very high density of extensional fractures, perhaps representing zones of localized hydrofracturing caused by sudden changes in hydrostatic pressures. Fault rocks are extremely rare in the drill core and the microfractures previously described as "microfaults" (Alt, Kinoshita, Stokking, et al., 1993) may actually be extension fractures. Some fractures that have been described from the lower dikes of Hole 504B during Legs 140 and 148 consist of millimeter-scale cataclastic zones cemented by hydrothermal minerals. Such cementation of heavily fractured rocks by hydrothermal minerals is characteristic of oceanic faults in ophiolites. Uncemented fault rocks, however, are unlikely to be recovered by drilling, and thus their absence in the drill core does not necessarily mean that they are absent in the basement, especially when there is only 10% core recovery as in the lower half of Hole 504B.

SUMMARY

The massive, aphyric to phyric diabasic rocks in the lower sheeted dike complex in Hole 504B mainly contain veins and fractures-microfractures with rare occurrences of igneous contacts and cataclastic zones. Heterogeneously distributed veins are composed mainly of actinolite, chlorite ± actinolite, and chlorite minerals and show two groups of orientations. One group consists of veins that strike east-southeast with steep dips; these veins occur parallel to the dike azimuth but perpendicular to the spreading direction along the Costa Rica Rift. The second group includes veins with a north-northeast strike that may represent dike-orthogonal, cooling fractures. Veins show evidence for internal deformation at depths from 2057 to 2090 mbsf but do not display any displacement and/or shearing along and across their boundaries. They are interpreted to have formed mostly as extensional mode I fractures. FMS images do not pick up the veins.

Microfractures with lineated surfaces are abundant throughout the core and are quite densely spaced in certain intervals at depth (i.e., 2026–2052, 2103–2111 mbsf) in the hole. The majority of the oriented microfractures has steep dips (>70°) and east-northeast strikes with subhorizontal slickenline lineations; gently dipping microfractures display steeply plunging lineations. There is no evidence for displacement, shearing, and/or mineralization along these microfracture surfaces. Their distribution in the hole may be spatially associated with damage zones near faults or localized deformation zones. Incipient and well-developed open fractures show shallow and steep dips and are locally symmetric to the modern in situ stress field. They are interpreted as drilling-induced features. FMS images depict a persistent fracture set with an average strike and dip of 52°/56° northwest between 1900 and 2000 mbsf in the hole. This orientation is different from the orientation of the Costa Rica Rift axis and the modern horizontal principal stress directions. Subhorizontal fractures observed in the drill core do not appear in the FMS data (hence in the drill hole), suggesting that they are drilling induced. There are two zones of intense fracturing in the vicinity of 1930 and 2000 mbsf as depicted from FMS images and DLL porosity logs. The zone at 1930 mbsf is dominated by subhorizontal fractures, whereas the one at 2000 mbsf is dominated by vertical fractures. These zones display several domains with different dip directions. In general, fault rocks are rare in the drill core, and an unequivocal assignment of intensely fractured zones derived from FMS data to natural faults is highly interpretive.

Millimeter-scale cataclastic zones in the drill core are spatially associated with veins and chilled dike margins and are cemented by hydrothermal minerals. Three dike margins have steep (76°–88°) dips and are nearly parallel to the Costa Rica Rift axis.

The Hole 504B remains to be the deepest reference section through in situ oceanic crust and provides significant information on the structural architecture of intermediate-spread oceanic lithosphere. Future drilling and structural studies at Site 504B are most critical to decipher the nature of deformation encountered in the bottom of the hole during Leg 148 and to investigate the dike-gabbro boundary, which may occur just beneath this deformation zone at 2111.0 mbsf.

ACKNOWLEDGMENTS

This work was supported by JOI/USSAC grants to Y. Dilek and G.D. Harper. We thank M. Ayadi in Marseille for her help with the FMS data reduction and the staff of Institut Méditerranéen de Technologie in Marseille for their kind hospitality during our stay. Critical reviews by James Natland and Jack Casey were helpful in improving the paper.

REFERENCES

Adamson, A.C., 1985. Basement lithostratigraphy, Deep Sea Drilling Project Hole 504B. *In* Anderson, R.N., Honnorez, J., Becker, K., et al., *Init. Repts. DSDP,* 83: Washington (U.S. Govt. Printing Office), 121–127.

Agar, S.M., 1990. Fracture evolution in the upper ocean crust: evidence from DSDP Hole 504B. *In* Knipe, R.J., and Rutter, E.H. (Eds.), *Deformation Mechanisms, Rheology and Tectonics.* Geol. Soc. Spec. Publ. London, 54:41–50.

———, 1991. Microstructural evolution of a deformation zone in the upper ocean crust: evidence from DSDP Hole 504B. *J. Geodyn.,* 13:119–140.

Agar, S.M., and Marton, F.C., 1995. Microstructural controls on strain localization in ocean crust diabases: evidence from Hole 504B. *In* Erzinger, J., Becker, K., Dick, H.J.B., and Stokking, L.B. (Eds.), *Proc. ODP, Sci. Results,* 137/140: College Station, TX (Ocean Drilling Program), 219–230.

Allerton, S.A., McNeill, A.W., Stokking, L.B., Pariso, J.E., Tartarotti, P., Marton, F.C., and Pertsev, N.N., 1995. Structures and magnetic fabrics from the lower sheeted dike complex of Hole 504B reoriented using stable magnetic remanence. *In* Erzinger, J., Becker, K., Dick, H.J.B., and Stokking, L.B. (Eds.), *Proc. ODP, Sci. Results,* 137/140: College Station, TX (Ocean Drilling Program), 245–252.

Alt, J.C., Anderson, T.F., Bonnell, L., and Muehlenbachs, K., 1989. Mineralogy, chemistry, and stable isotopic composition of hydrothermally altered sheeted dikes: ODP Hole 504B, Leg 111. *In* Becker, K., Sakai, H., et al., *Proc. ODP, Sci. Results,* 111: College Station, TX (Ocean Drilling Program), 27–40.

Alt, J.C., Honnorez, J., Laverne, C., and Emmermann, R., 1986. Hydrothermal alteration of a 1 km section through the upper oceanic crust, Deep Sea Drilling Project Hole 504B: mineralogy, chemistry, and evolution of seawater-basalt interactions. *J. Geophys. Res.,* 91:10309–10335.

Alt, J.C., Kinoshita, H., Stokking, L.B., et al., 1993. *Proc. ODP, Init. Repts.,* 148: College Station, TX (Ocean Drilling Program).

Alt, J.C., Laverne, C., and Muehlenbachs, K., 1985. Alteration of the upper oceanic crust: mineralogy and processes in Deep Sea Drilling Project Hole 504B, Leg 83. *In* Anderson, R.N., Honnorez, J., Becker, K., et al., *Init. Repts. DSDP,* 83: Washington (U.S. Govt. Printing Office), 217–247.

Alt, J.C., and the Leg 148 Scientific Party, 1993. Probing the Layer 2/Layer 3 transition in Hole 504B, ODP Leg 148. *Eos,* 74:645.

Anders, M.H., and Wiltschko, D.V., 1994. Microfracturing, paleostress and the growth of faults. *J. Struct. Geol.,* 16:795–815.

Anderson, R.N., Honnorez, J., Becker, K., et al., 1985. *Init. Repts. DSDP,* 83: Washington (U.S. Govt. Printing Office).

Becker, K., Sakai, H., Adamson, A.C., Alexandrovich, J., Alt, J.C., Anderson, R.N., Bideau, D., Gable, R., Herzig, P.M., Houghton, S.D., Ishizuka, H., Kawahata, H., Kinoshita, H., Langseth, M.G., Lovell, M.A., Malpas, J., Masuda, H., Merrill, R.B., Morin, R.H., Mottl, M.J., Pariso, J.E., Pezard, P.A., Phillips, J.D., Sparks, J.W., and Uhlig, S., 1989. Drilling deep into young oceanic crust, Hole 504B, Costa Rica Rift. *Rev. Geophys.,* 27:79–102.

Becker, K., Sakai, H., et al., 1988. *Proc. ODP, Init. Repts.,* 111: College Station, TX (Ocean Drilling Program).

Bergman, E.A., 1986. Intraplate earthquakes and the state of stress in oceanic lithosphere. *Tectonophysics,* 132:1–35.

Cann, J.R., Langseth, M.G., Honnorez, J., Von Herzen, R.P., White, S.M., et al., 1983. *Init. Repts. DSDP,* 69: Washington (U.S. Govt. Printing Office).

Cox, S.F., and Etheridge, M.A., 1983. Crack-seal fibre growth mechanisms and their significance in the development of oriented layer silicate microstructures. *Tectonophysics,* 92:147–170.

Detrick, R.S., Collins, J., Stephen, R., and Swift, S., 1993. Evidence that the seismic Layer 2/3 boundary occurs above the dike/gabbro transition in Hole 504B. *Eos,* 74:645.

———, 1994. *In situ* evidence for the nature of the seismic layer 2/3 boundary in oceanic crust. *Nature,* 370:288–290.

Dick, H.J.B., Erzinger, J., Stokking, L.B., et al., 1992. *Proc. ODP, Init. Repts.,* 140: College Station, TX (Ocean Drilling Program).

Engelder, T., 1987. Joints and shear fractures in rock. *In* Atkinson, B.K. (Ed.), *Fracture Mechanics of Rock:* London (Acad. Press), 27–69.

Etheridge, M.A., Wall, V.J., Cox, S.F., and Vernon, R.H., 1984. High fluid pressures during regional metamorphism and deformation: implications for mass transport and deformation mechanisms. *J. Geophys. Res.,* 89:4344–4358.

Hobart, M.A., Langseth, M.G., and Anderson, R.N., 1985. A geothermal and geophysical survey on the south flank of the Costa Rica Rift: Sites 504 and 505. *In* Anderson, R.N., Honnorez, J., Becker, K., et al., *Init. Repts. DSDP,* 83: Washington (U.S. Govt. Printing Office), 379–404.

Honnorez, J., Alt, J.C., Honnorez-Guerstein, B.-M., Laverne, C., Muehlenbachs, K., Ruiz, J., and Saltzman, E., 1985. Stockwork-like sulfide mineralization in young oceanic crust: Deep Sea Drilling Project Hole 504B. *In* Anderson, R.N., Honnorez, J., Becker, K., et al., *Init. Repts. DSDP,* 83: Washington (U.S. Govt. Printing Office), 263–282.

Honnorez, J., Laverne, C., Hubberten, H.-W., Emmermann, R., and Muehlenbachs, K., 1983. Alteration processes in Layer 2 basalts from Deep Sea Drilling Project Hole 504B, Costa Rica Rift. *In* Cann, J.R., Langseth, M.G., Honnorez, J., Von Herzen, R.P., White, S.M., et al., *Init. Repts. DSDP,* 69: Washington (U.S. Govt. Printing Office), 509–546.

Kanaori, Y., Yairi, K., and Ishida, T., 1991. Grain boundary microcracking of granitic rocks from the northeastern region of the Atotsugawa fault, central Japan: SEM backscattered electron images. *Eng. Geol.,* 30:221–235.

Kulander, B.R., Dean, S.L., and Ward, B.J., Jr., 1990. *Fractured Core Analysis: Interpretation, Logging, and Use of Natural and Induced Fractures in Core.* Methods Explor. Ser., 8: Tulsa, OK (AAPG).

Lüthi, S.M., and Banavar, J.R., 1988. Application of borehole images to three-dimensional geometric modeling of eolian sandstone reservoirs, Permian Rotliegende, North Sea. *AAPG Bull.,* 72:1074–1089.

Morin, R.H., Anderson, R.N., and Barton, C.A., 1989. Analysis and interpretation of the borehole televiewer log: information on the state of stress and the lithostratigraphy at Hole 504B. *In* Becker, K., Sakai, H., et al., *Proc. ODP, Sci. Results,* 111: College Station, TX (Ocean Drilling Program), 109–118.

Morin, R.H., Newmark, R.L., Barton, C.A., and Anderson, R.N., 1990. State of lithospheric stress and borehole stability at Deep Sea Drilling Project Site 504B, eastern Equatorial Pacific. *J. Geophys. Res.,* 95:9293–9303.

Newmark, R.L., Anderson, R.N., Moos, D., and Zoback, M.D., 1985a. Sonic and ultrasonic logging of Hole 504B and its implications for the structure, porosity, and stress regime of the upper 1 km of the oceanic crust. *In* Anderson, R.N., Honnorez, J., Becker, K., et al., *Init. Repts. DSDP,* 83: Washington (U.S. Govt. Printing Office), 479–510.

Newmark, R.L., Zoback, M.D., and Anderson, R.N., 1985b. Orientation of in situ stresses near the Costa Rica Rift and Peru-Chile Trench, Deep Sea Drilling Project Hole 504B. *In* Anderson, R.N., Honnorez, J., Becker, K., et al., *Init. Repts. DSDP,* 83: Washington (U.S. Govt. Printing Office), 511–514.

Petit, J.P., 1987. Criteria for the sense of movement on fault surfaces in brittle rocks. *J. Struct. Geol.,* 9:597–608.

Pezard, P.A., and Anderson, R.N., 1989. Morphology and alteration of the upper oceanic crust from in-situ electrical experiments in DSDP/ODP Hole 504B. *In* Becker, K., Sakai, H., et al., *Proc. ODP, Sci. Results,* 111: College Station, TX (Ocean Drilling Program), 133–146.

Pollard, D.D., and Aydin, A., 1988. Progress in understanding jointing over the past century. *Geol. Soc. Am. Bull.,* 100:1181–1204.

Ramsay, J.G., 1980. The crack-seal mechanism of rock deformation. *Nature,* 284:135–139.

Ramsay, J.G., and Huber, M.I., 1983. *The Techniques of Modern Structural Geology* (Vol. 1): *Strain Analysis:* London (Acad. Press).

Roeckel, T., Natau, O., and Dietrich, H.-G., 1992. Core reorientation by comparison of core instabilities and borehole instabilities. *In* Emmermann, R., Dietrich, H.-G., et al., *KTB Hauptbohrung, Results of Geoscientific Investigation in the KTB Field Laboratory, 0–6000 m.* KTB Rep. 92-2:F1–F17.

Scholz, C.H., Dawers, N.H., Yu, J.-Z., and Anders, M.H., 1993. Fault growth and fault scaling laws: preliminary results. *J. Geophys. Res.,* 98:21951–21961.

Tartarotti, P., Allerton, S.A., and Laverne, C., 1995. Vein formation mechanisms in the sheeted dike complex from Hole 504B. *In* Erzinger, J., Becker, K., Dick, H.J.B., and Stokking, L.B. (Eds.), *Proc. ODP, Sci. Results,* 137/140: College Station, TX (Ocean Drilling Program), 231–244.

Wolter, K.E., Roeckel, T., et al., 1990. Core disking in KTB drill cores and the determination of the in-situ stress orientation. *In* Emmermann, R., Dietrich, H.-G., et al. (Eds.), *Pilot Hole, Results of Geoscientific Investigation in the KTB Field Laboratory, 0–4000.1 m.* KTB Rep. 90-8:G1–G13.

Date of initial receipt: 18 August 1994
Date of acceptance: 13 March 1995
Ms 148SR-131